Mapana – Journal of Sciences
2026, Vol. 25, No. 1, *19-32*
ISSN 0975-3303 | https://doi.org/10.12723/mjs.76.2

Electrochemically active chitosan loaded PbS NPs with effective degradation against methylene blue dye and *E. coli* bacteria disinfection

N. Manjula*, N. Arunkumar*, A.R. Balu*, S. Ganesan†, K. Devendran*, M. Sriramraj*, A. Vinith*, V. Rajamani*

Abstract

This paper reports the photocatalytic, electrochemical and antibacterial properties of cubic crystal-structured pure PbS and chitosan, a cationic polymer loaded PbS NPs synthesized by the chemical precipitation method. Chitosan loading decreased the crystallite size of pure PbS from 34 to 27 nm. The occurrence of π-plasmon with chitosan loading shifted the absorption edge of pure PbS to higher wavelength side and decreased the band gap from 1.94 to 1.87 eV. PbS's degradation efficiency against MB dye under visible light with chitosan loading increased from 83.2 to 92 %, and the degradation rate constants were 0.0178 and 0.0241 $min^{-1,}$ respectively, for pure PbS and chitosan-loaded PbS NPs. Specific capacitance of pure PbS increased from 71.3 to 97.8 F/g with chitosan loading due to the synergetic effect between PbS and chitosan bio-polymer. With the presence of free hydroxyl groups in chitosan, more ROS are generated in the chitosan-loaded PbS NPs, resulting in enhanced antibacterial activity.

Keywords: Chitosan; cationic polymer; XRD; photodegradation; bacterial inhibition; specific capacitance

1. Introduction

Transition metal chalcogenides exhibit excellent photo-electron transformation properties, especially at the nanoscale [1]. Among the metal

* Department of Physics, AVVM Sri Pushpam College (Affiliated to Bharathidasan University, Tiruchirappalli), Poondi, Tamilnadu, India; manjula_msc@rediffmail.com; aroon5465@gmail.com; arbalu757@gmail.com; devendran2187@gmail.com; Sriramrajphysics@gmail.com; vinithakt2000@gmail.com; Sruthirithi14@gmail.com

† Department of Zoology and Biotechnology, AVVM Sri Pushpam College (Affiliated to Bharathidasan University, Tiruchirappalli), Poondi, Tamilnadu, India; ganesanmolbio@gmail.com

chalcogenides of the IV-VI group, lead sulfide (PbS) has a cubic crystalline lattice with fcc unit cell, showing both n-type and p-type conductivity characteristics [2]. When in its bulk state and undergoing direct transition, it possesses a narrow band gap of 0.41 eV. Among the characteristics of this material are a larger excitonic Bohr radius, high absorption coefficient and smaller effective electronic and protonic masses [3]. As a result of its photo-induced conductive properties, PbS finds applications in solar cells, infrared emitters, diodes, gas sensors, optical data storage, etc [4]. Due to its nonlinear optical behaviour, PbS is potentially useful in electroluminescent devices like LEDs and optical switches [5]. PbS's robust structure and mechanical stability make it an ideal material in pseudo capacitors [6]. PbS in the nanoregime showed excellent photocatalytic and antimicrobial properties [7, 8].

Although PbS has many potential uses, it isn't always the most efficient material for devices made from it due to issues like lower band gap, surface oxidation instability and hydroxyl motifs that encourage trap states. PbS's intrinsic properties and disadvantages could be addressed by coupling with coagulants which offer immense chemical and mechanical modifications. Among the various coagulants, chitosan is a non-toxic linear high molecular weight cationic polymer which can increase the surface charge and bonding sites of PbS, improving its electrochemical, catalytic and antibacterial properties. Chitosan improving CuS:Ni and CuS:Co's electrochemical, nonlinear optical, magnetic and antibacterial properties has been reported earlier [9,10]. Herein PbS and chitosan loaded PbS NPs are synthesized by chemical precipitation and comparison has been made on their electrochemical, photocatalytic and antibacterial properties.

2. Experimental

By using lead nitrate, thiourea each of 0.1M as precursor salts and chitosan (2% (2.55 gm), optimized value), PbS and chitosan loaded PbS NPs are synthesized.

2.1. PbS (LS) NPs - Synthesis

In 135 mL water, the precursor salts (4.998 g of lead nitrate & 1.142 g of thiourea) were dissolved. To this solution, 15 mL liquid NH_3 was added and stirred for 5 h. Precipitates settled were filtered, washed, calcined for 2 h at 350^{o}C and crushed to form LS NPs.

2.2. Synthesis of chitosan-loaded PbS (CLS) NPs

To synthesize CLS NPs, 2.55 gm of chitosan was added to the solution prepared as discussed in Section 2.1. The pH value was raised to 10 by adding 15 mL liquid NH_3. After being aged for 4 hours, solids settled down

and CLS NPs were synthesized after calcination and crushing.

2.3. Characterization

Diffraction data of LS and CLS NPs were performed using a diffractometer PW 340/60. Surface was analyzed using HITACHI S-3000 H microscope. Optical band gap values were calculated from the absorbance spectra using λ-35 spectrophotometer. Functional group analysis and photoluminescence spectra were obtained using RX-1 and Varian cary spectrophotometers.

2.4. Photocatalytic test

LS and CLS catalysts were tested against methylene blue using white light with an intensity 100 mW/cm^2. To perform the photocatalytic test, 10 mL dye solution was taken by dissolving 0.0025 M (0.8 g/L) MB dye. To this solution, 0.4 g/L of LS and CLS NPs was added and exposed to light with continuous stirring. At 660 nm, MB's absorption spectra were monitored by centrifuging the catalysts every 20 min.

2.5. Electrochemical studies

CV studies were feasible through EG & G, Model:273 A work station. Counter, reference and working electrodes are platinum, Ag/AgCl, LS and CLS NPs with electrolyte being $Na_2S_2O_3$.

2.6. Antibacterial test

E. coli bacteria cultured on Muller-Hinton agar was tested for antibacterial potency of LS and CLS NPs. To wells created (6 mm diameter), 20 µg/mL of NPs dissolved in 20, 40, 60 and 80 µL DMSO was placed and incubated for 24 h at 37^oC. Measuring zones of inhibition (ZOI) values, antibacterial activity was evaluated.

3. Results and Discussion

3.1. XRD

LS and CLS NPs' XRD patterns are illustrated in Figure 1. Diffraction peaks observed at 2θ values 26.12°, 30.23°, 43. 22°, 51.13°, 53.59°, 62.65° and 71.03° correspond to (111), (200), (220), (311), (222), (400) and (331) planes.

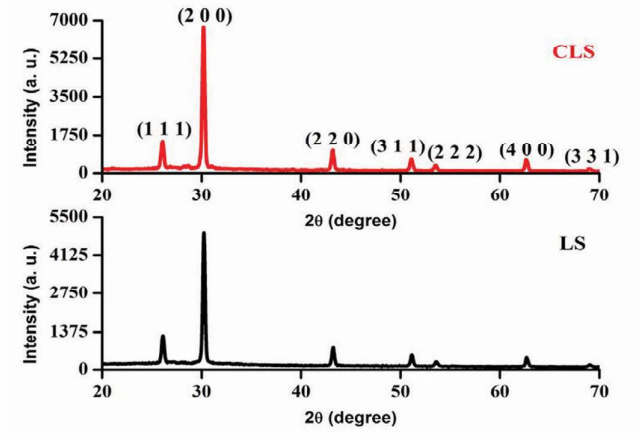

Figure 1: LS and CLS's XRD patterns

All the diffraction peaks matches with JCPDS No. 65-0592 which corresponds to cubic PbS [14]. With chitosan loading, the LS peaks' positions moved to higher Bragg angles. Furthermore, the sharpness of the diffraction peaks of LS decreased with chitosan loading indicating that chitosan loading deteriorated the crystallinity of pure PbS which might be due to chitosan's molecular chain absorption on the surface of PbS [XI]. Based on the Scherrer formula, $D = \frac{0.9\,\lambda}{\beta\,cos\theta}$ (β - full width at half maximum, λ=1.5406 Å and θ-Bragg's angle), the crystallite sizes were 34 and 27 nm, respectively for LS and CLS.

3.2. *SEM*

Surfaces of both LS and CLS are covered with grains uniformly distributed, as evinced from the SEM images (Figure 2). Few pin holes and empty sites are visible for LS; which got minimized in CLS. For LS, grains aggregate; for CLS, highly defined boundaries are observed. Thus, chitosan loading improved PbS's surface morphology.

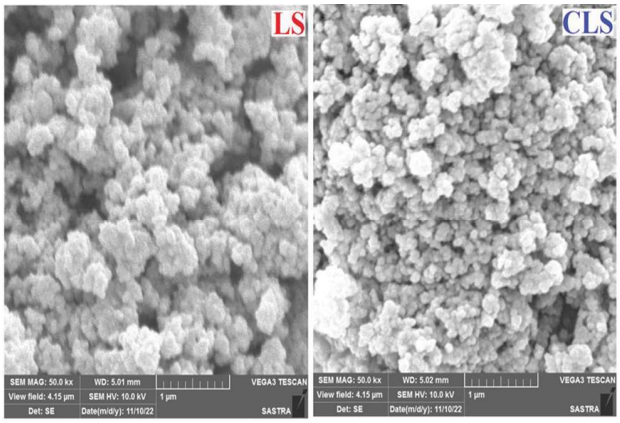

Figure 2: LS and CLS's SEM images

Agglomerated grains are seen in both LS and CLS's TEM images (Figure 3). Few spherical and cubic-shaped grains are seen for CLS. The black coating observed indicates the capping of chitosan over PbS. The grain sizes were 72 and 56 nm for LS and CLS.

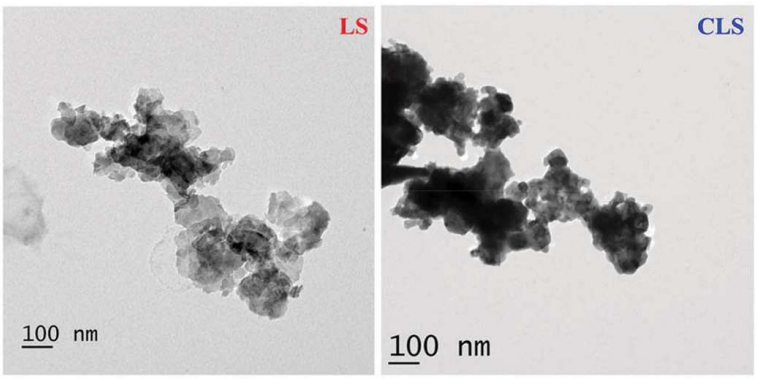

Figure 3: LS and CLS's TEM images

3.3. *FTIR*

OH stretching vibrations occur at 3388, 1633 for LS (Figure 4) and at 3509, 1714, 1623 cm^{-1} for CLS. C–H bond stretching occurs at 2921 for LS, at 2923 for CLS and at 2852 cm^{-1} for both samples.

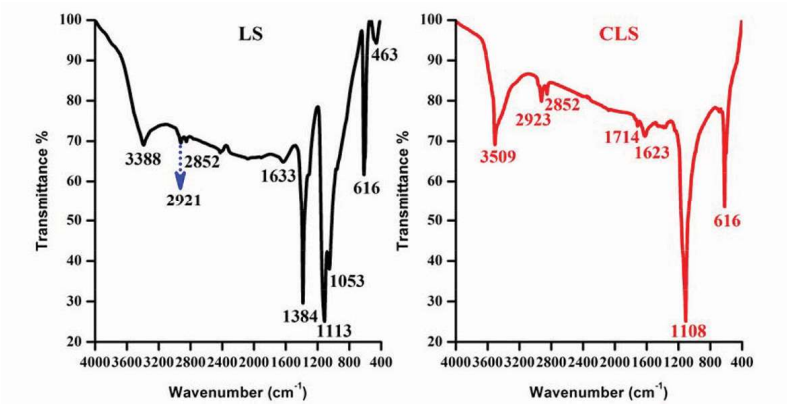

Figure 4: LS and CLS's FTIR spectra

LS showed a C–O–H stretching peak at 1384 cm^{-1} related to carboxyl groups. Antisymmetric stretching of SO_4 occurs at 1113 for LS and at 1108 cm^{-1} for CLS. C–C bonding occurs at 1053 for LS and peaks related to PbS occur at 616 cm^{-1} for both LS and CLS and at 463 for LS [7].

3.4. Optical studies

Absorption edge of CLS shifts towards the higher wavelength side (Figure 5(a)) as a result of the occurrence of the π-plasmon with chitosan loading [18]. The band gap energies (E_g) were calculated via Tauc plot (Figure 5(b)) using the equation:

$$(ahv)^2 = (hv\text{-}E_g) \qquad (1)$$

The E_g values are 1.94 and 1.87 eV, for the LS and CLS NPs. CLS's reduced band gap results from the formation of impurity sub-band near the valence band due to the synergistic interaction between PbS and chitosan.

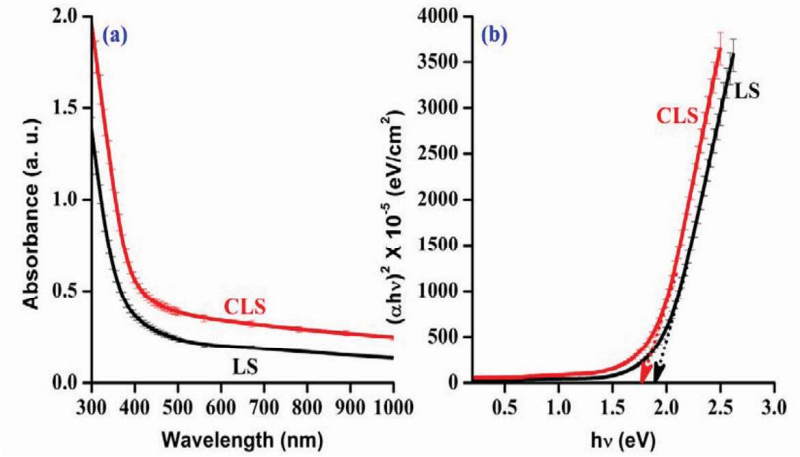

Figure 5: LS and CLS's a) Absorbance spectra and b) Tauc plots

3.5. PL studies

Quantum confined excitonic emission occurs at 360 and 380 nm for LS and at 355 nm for CLS as seen in the Gaussian fitted PL spectra (Figure 6).

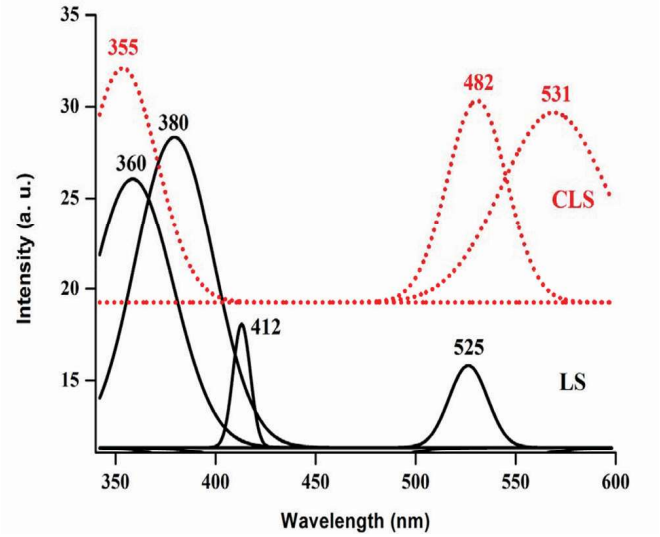

Figure 6: LS and CLS's PL spectra

Interstitial sulfur lattice defects account for the peaks at 412 for LS and 482 nm for CLS. As seen in CLS, the peak at 482 nm appeared broad, possibly due to the radiative recombination of self-trapped excitons. The surface trap-induced peaks at 525 and 531 nm for LS and CLS are due to

electron recombination with holes in the valence band, due to sulfur vacancy trapping.

3.6. Photocatalytic activity

In order to confirm the photodegradation processes, the absorbance was measured and plotted (Figure 7). Continuously decreasing absorbance indicates degradation of MB.

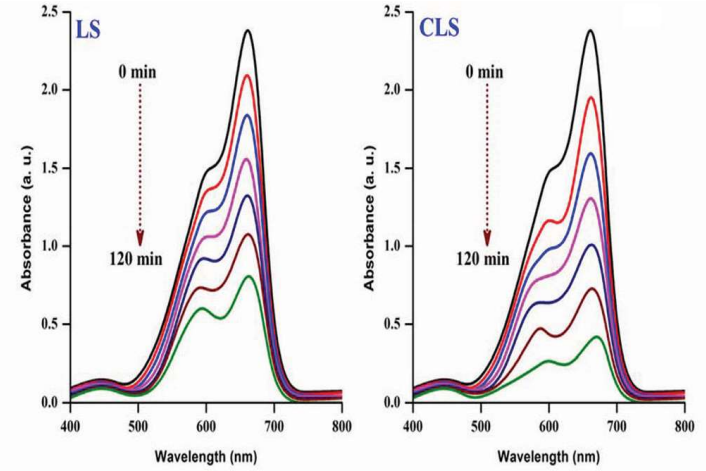

Figure 7: Absorbance spectra of LS and CLS catalysts

The dye solution showed negligible degradation when irradiated without catalysts, confirming the stability of the MB dye (Figure 8). Degradation efficiency increased with increasing irradiation time with LS and CLS catalysts. The degradation efficiencies were 83.2 and 92 % after 100 min light irradiation for the LS and CLS catalysts, respectively (Figure 9). A possible explanation for the increased degradation efficiency observed for the CLS catalyst may be the decoration of chitosan, which provides a pathway for electron transfer [21]. By providing fewer hindered paths, chitosan loading increase the surface area of CLS, therefore improving dye adsorption [22].

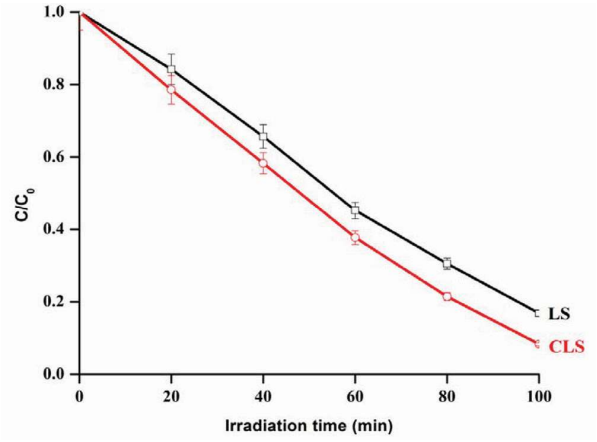

Figure 8: Plots of (C/C_0) vs. reaction time

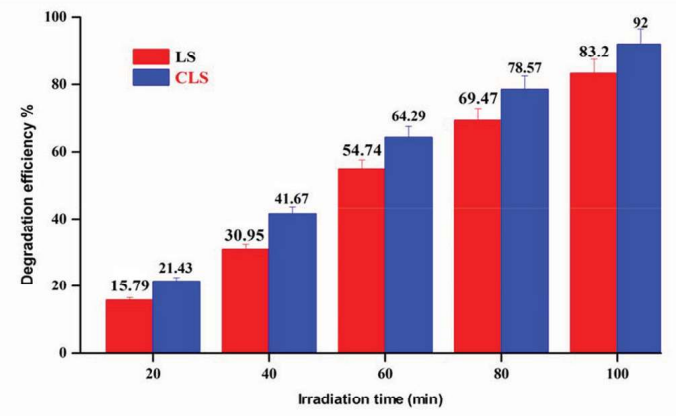

Figure 9: Degradation efficiencies of LS and CLS catalysts

The first order reaction kinetics of photodegradation was studied using the equation:

$$-\ln(C/C_0) = kt \qquad (2)$$

From the kinetics plots (Figure 10), the rate constants (k) were 0.0178 and 0.0241 min^{-1} for LS and CLS catalysts, respectively.

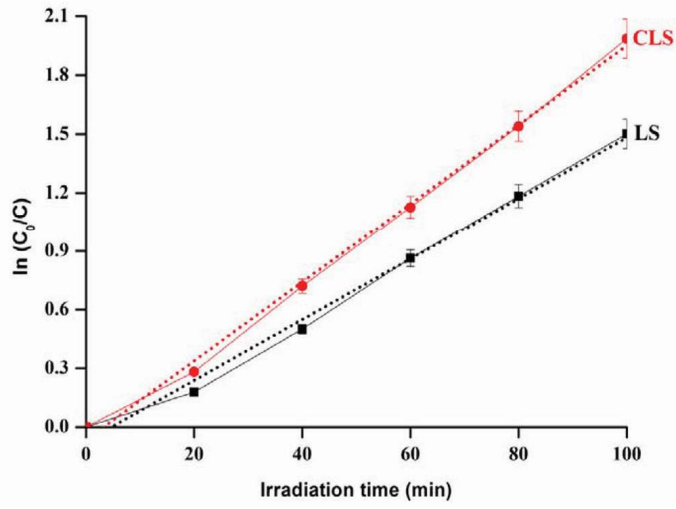

Figure 10: Plots of ln(C0/C) vs. irradiation time

The regression coefficient (R^2) and standard error values are 0.99126, 0.99584 and 0.03952, 0.03529 for LS and CLS samples. MB photodegradation was high for the CLS catalyst, as indicated by its high 'k' value. The breakdown of MB dye with a) LS and b) CLS catalysts is shown in Figure 11. For both LS and CLS catalysts, electrons from the VB are excited to CB when the dye solution with the catalysts is exposed under visible light. The excited electrons react with adsorbed O_2 molecules to form O_2^{*-} radicals, and the holes react with OH^- present in the aqueous solution to form OH^* radicals. MB dye molecules

are decomposed into CO_2, H_2O and other small molecules by these radicals. e^--h^+ pairs recombinate faster in pure PbS, slowing down the degradation process. PbS loaded with chitosan enhanced the photodegradation of dye by prolonging the recombination process of e^--h^+ pairs. Chitosan polymer acts as an electron acceptor and transporter in CLS due to its nice interfacial contact with PbS NPs. The delay in the recombination time of photogenerated e^--h^+ pairs increases the density of carriers in dye solution containing CLS catalyst which further reacts with O_2 and OH^- forming more O_2^{*-} and OH^* radicals degrading MB dye relatively higher than pure PbS.

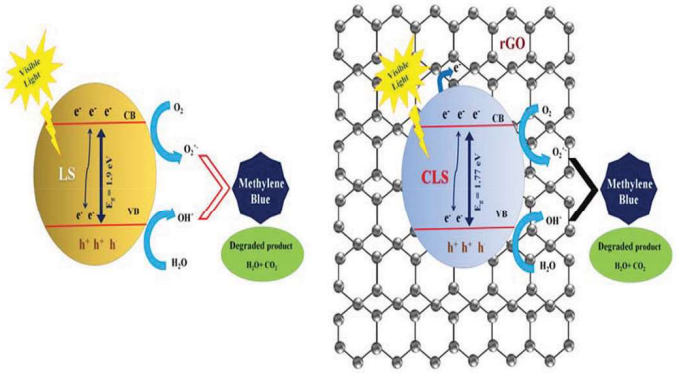

Figure 11: Photocatalytic scheme involved in a) LS and b) CLS catalysts

To ascertain the radicals involved in the degradation of MB by the CLS catalyst, scavenger tests were done using potassium iodide (PI), benzoquinone (BQ), and isopropanol (IPA) as scavengers for h^+, O_2^{*-} and OH^*, respectively. Compared to PI, enhanced degradation efficiency was realized with BQ and IPA scavengers, confirming that both OH^* and O_2^{*-} are the main radicals that degraded MB dye molecules.

3.7. Electrochemical

CV curves of LS and CLS NPs are shown in Figures 12 and 13. Scan rates of 25, 50, 75 and 100 mV/s was used for conducting the electrochemical studies.

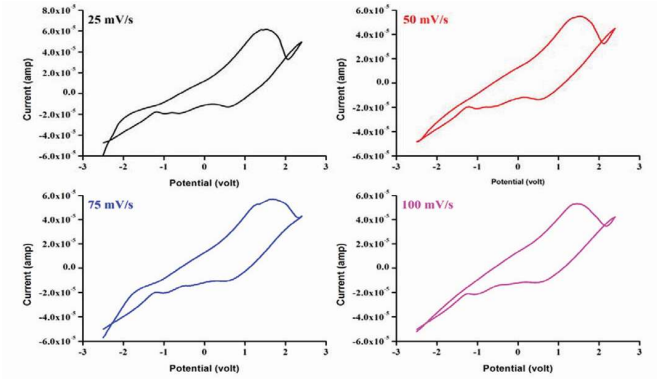

Figure 12: CV curves of LS

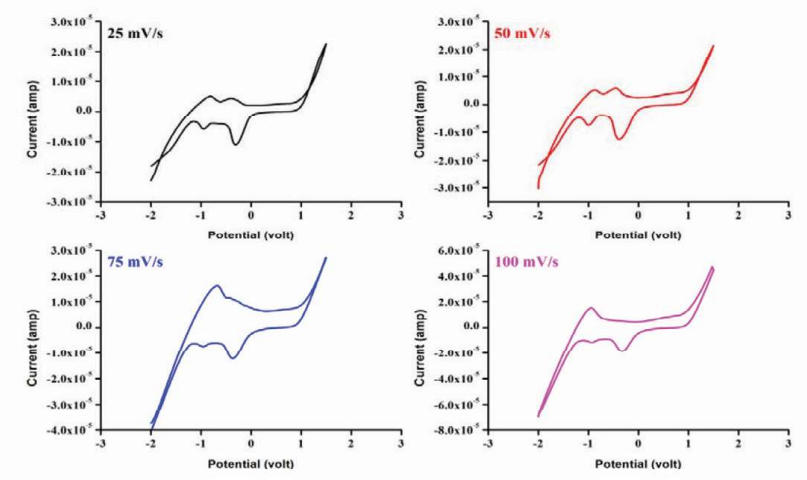

Figure 13: CV curves of CLS

As for LS, CV curves were asymmetrical, while for CLS sharp reduction-oxidation peaks were observed which is creditable to chitosan's addition. Inclusion of chitosan in PbS can provide multidimensional electron transport pathways and result in the accumulation of charges on its surface [23]. Observed oxidation peaks are a result of the oxidation of Pb to Pb^{2+}, while the reduction peaks are caused by the decomposition of the electrolyte and the reduction of Pb^{2+} to Pb.

$$Pb \rightarrow Pb^{2+} + 2e^{-}$$
$$Pb^{2+} + 2e^{-} \rightarrow Pb$$

Electrochemical formation of S occurs when $Na_2S_2O_3$ decomposes under acidic conditions.

$$S_2O_3^{2-} + 2H^{+} \rightarrow S + SO_2 + H_2O$$

PbS formation is represented by the electrochemical reaction:

$$Pb^{2+} + S + 2^{e-} \rightarrow PbS$$

CLS's CV surface area increased with an increase in scan rate up to 75 mV/s, and then it slightly decreased. Enhanced surface area at 75 mV/s facilitates Faradaic reaction at the electrode-electrolyte interface. Even when scan rates increase, the CV curves remain consistent in shape, which is manifested by greater reversibility of redox reactions [24]. Specific capacitance (C_S) values calculated using the formula, $C_S = \frac{A}{smV}$ were 71.3 and 97.8 F/g for LS and CLS, respectively. CLS's improved surface shape allows for optimal ion insertion and desorption for the storage mechanism, resulting in a maximum C_S value. Furthermore, the smaller ion crystallites will reduce the route length, making it easier to achieve high charge/discharge rates. Furthermore, C_S rises owing to improved interfacial efficacy between CLS and the electrolyte.

EIS data helped to clarify the interfacial charge transfer process occurring between the electrode and electrolyte (Figure 14). LS and CLS show a semicircular pattern in high-frequency domain and a linear segment in low-frequency domain. Chitosan loading causes LS's semicircle diameter to decrease, resulting in decreased polarization and low charge transfer resistance (R_{ct}), which speeds up ion diffusion in the electrolyte. The R_{ct} values were 29.3 and 12.4 x 10^3 Ω respectively for LS and CLS. CLS's lowest charge transfer resistance rating confirmed its promise as a supercapacitor.

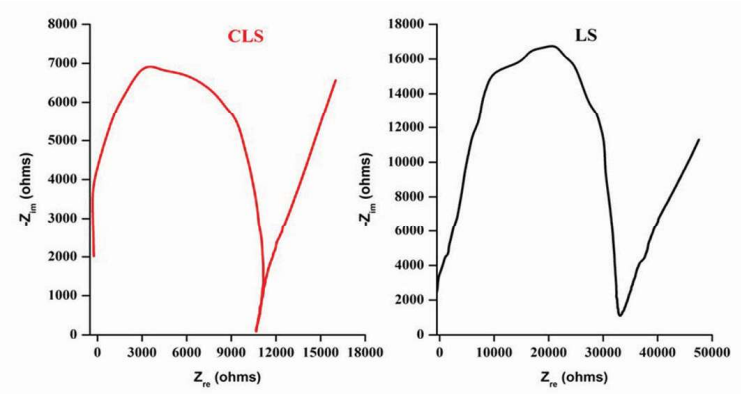

Figure 14: Nyquist plots of CLS and LS

3.8. Antibacterial

The antibacterial activities of LS and CLS NPs (2 mg dissolved in 20, 40, 60 and 80 µL DMSO) against *E. coli* bacteria are illustrated in Figure 15, and the zones of inhibition (ZOI) values are compiled in Table 1.

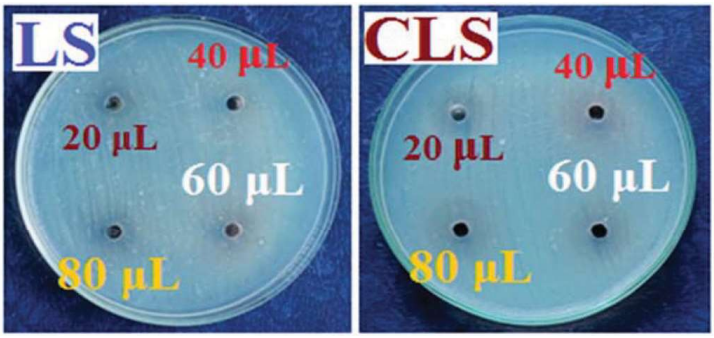

Figure 15: Antibacterial activities of LS and CLS

Concentration (µL)	Zone of inhibition (mm)	
	LS	CLS
20	3	4
40	5	7
60	10	14
80	13	17

Table 1: ZOI values observed for LS and CLS NPs

Higher antibacterial performance is observed for the CLS composite. PbS and chitosan work against bacteria by releasing Pb^{2+} ions that attach to the thiol groups of proteins and enzymes to destabilize their cellular walls and membranes. Due to the perforation of the bacteria's cellular wall and membrane, LS and CLS NPs would diffuse into the bacteria's interior to cause further DNA damage [25]. ROS (O_2^{*-}, OH^*, H_2O_2) production significantly contributes to the antibacterial property of LS and CLS NPs. Nucleic acids, lipids, proteins, DNA, and carbohydrates are all harmed by ROS. ROS cause severe oxidative stress in bacteria, preventing cell division and growth by damaging several biological functions [19]. Differences in the antibacterial performance of LS and CLS NPs are influenced by several factors, such as ROS production ability, improved surface morphology, decreased band gap, etc. The activation of the mitochondrial pathway by chitosan inclusion results in increased ROS generation and bacterial death [26]. Chitosan in the CLS sample kills bacteria by initiating a chain reaction of biological processes. By preventing PbS NPs from aggregating, chitosan prolongs the CLS's antibacterial activity [27]. Pure PbS has the ability to get easily agglomerated which decreases its interaction with bacteria, and hence it possess low antibacterial activity than the chitosan-loaded PbS. Chitosan-PbS combination compensates for PbS's disadvantages due to its superior specific surface area and the presence of free hydroxyl groups. Consequently, CLS would be more dispersible and agglomeration would be prevented, and hence enhanced antibacterial activity was realised.

4. Conclusion

Pure PbS and chitosan loaded PbS NPs were synthesized by chemical precipitation method. Analyses were performed on the synthesized samples to determine their structural, optical, photocatalytic, electrochemical, and antibacterial properties. Crystallite size of PbS decreased from 34 nm to 27 nm with chitosan loading. SEM images confirmed the presence of grains with well-defined boundaries for CLS. Degradation efficiencies were found to be 83.2 and 92 % for LS and CLS catalysts against MB dye under visible light after 100 min irradiation time. Increased degradation efficiency observed for CLS confirmed its potential to be an effective catalyst against the degradation of toxic organic dyes. PbS exhibits an improved antimicrobial activity when loaded with chitosan, which confirmed its efficacy as an antimicrobial agent. Increased specific capacitance realized for the chitosan loaded sampled confirmed its utility as an effective pseudocapacitor. Thus, chitosan loaded PbS could be a promising visible light driven photocatalyst for catalytic, pseudocapacitor for electrochemical and antimicrobial agent for biomedical applications. In future, other coagulants could be tried to improve the degradation efficiency, specific capacitance and antimicrobial properties of PbS better than chitosan.

Conflict of Interest: No conflict of interest exists in the article.

Authors' contributions:

Conceptualization - A.R. Balu; Methodology – N. Manjula; Formal analysis and investigation – M. Sriramraj; Writing – original draft preparation – N. Arunkumar; Writing – review and editing – A.R. Balu; Funding acquisition – K. Devendran, S. Ganesan; Interpretation of data – V. Rajamani, A. Vinith.

All the authors read and approved the final manuscript.

Funding

The authors confirm that they received no grants, funds, or other forms of assistance in preparing this manuscript."

Acknowledgements

For the FTIR studies, we thank Mr. Vincent of St. Joseph's College, Trichy.

References

[1]. A.S. Cuharuc, L.L. Kulyuk, R.I. Lascova, A.A. Mitioglu and A.I. Dikusar, Surf. Eng. Appl. Electrochem. **48**, 193 (2012). https://doi.org/10.3103/S1068375512030040

[2]. A. Zafar, K.S. Ahmad, S.B. Jaffri and M. Sohail, Phosphorus, Sulfur, Silicon Relat. Elem. **196**, 36 (2020). https://doi.org/10.1080/10426507.2020.1799371

[3]. B. Altiokka, Arab J. Sci. Eng. **40**, 2085 (2015). https://doi.org/10.1007/s13369-015-1680-3

[4]. Z.A. Motlagh and M.A. Araghi, Semicond. Sci. Technol. **31**, 025017 (2016). https://doi.org/10.1088/0268-1242/31/2/025017

[5]. K.V. Chandekar, F.H. Alkallas, A.B.G. Trabelsi, M. Shkir, J. Hakami, A. Khan, H.E. Ali, N.S. Awwad and S. AlFaify, Physica B **641**, 414099 (2022). https://doi.org/10.1016/j.physb.2022.414099

[6]. S. Majumder, S. Karade, R. Kumar, M. Gu, B.R. Sankapaland K.H. Kim, J. Alloys Compd. **906**, 164323 (2022). https://doi.org/10.1016/j.jallcom.2022.164323

[7]. M. Suganya and A.R. Balu, Mater. Sci. Poland. **35**, 322 (2017). https://doi.org/10.1515/msp-2017-0046

[8]. A. Mohammadi, M. Barikani, A.H. Doctorsafaei, A.P. Isfahani, E. Shams and B. Ghalei, Chem. Eng. J. **349**, 466 (2018). https://doi.org/10.1016/j.cej.2018.05.111

[9]. M.Karthika, A.R.Balu, M.Suganya, S.Chitradevi, M.Sriramraj, K.Devendran, G.Vinitha, Z.Delci, S.Balamurugan, Nano **3,** 2350014 (2023). https://doi.org/10.1142/S1793292023500145

[10]. M.Karthika, A.R.Balu, G.Vinitha, Z.Delci, M.Suganya, S.Chitradevi, K.Devendran, M.Sriramraj, Ceram. Int. **49,** 17806-17817 (2023) https://doi.org/10.1016/j.ceramint.2023.02.146

[11]. B.S. Kim, D.C.J. Neo, B. Hou, J.B. Park, Y. Cho and N. Zhang, ACS Appl. Mater. Interfaces **8,** 13902 (2016).https://doi.org/10.1021/acsami.6b02544

[12]. A.R. Lara-Canche, D.F. Garcia-Gutierrez, N. Torres-Gomez, J.E. Reyes-Gonzalez, D. Bahena-Uribe, S. Sepulveda-Guzman, I. Hernandez-Calderon and D.I. Garcia-Gutierrez, Nanotechnol. **29,** 32 (2021).10.1088/1361-6528/abc209

[13]. S. Ahn, H. Chung, W. Chen, M.A. Moreno-Gonzalez and O.Vazquez-Mena, J. Chem. Phys. **151,** 234705 (2019). https://doi.org/10.1063/1.5132562

[14]. N.F. Shaafi, S.K. Muzakir, S.B. Aziz, M.F. Zamani Kadir and S. Thanakodi, J. Alloys Compnd. **864**, 158117 (2021). https://doi.org/10.1016/j.jallcom.2020.158117

[15]. Q. Li, B. Guo, J. Yu, J. Ran, B. Zhang, H. Yan and J.R. Gong, J. Am. Chem. Soc. **133,** 10878 (2011). https://doi.org/10.1021/ja2025454

[16]. X. Fu, Y. Zhang, P. Cao, H. Ma, P. Liu, L. He, J. Peng, J. Li and M. Zhai, *Rad. Phys. Chem.* **123,** 79 (2016). https://doi.org/10.1016/j.radphyschem.2016.02.016

[17]. J. Liu, H. Bai, Y. Wang, Z. Liu, X. Zhang and D.D. Sun, Adv. Funct. Mater. **20**, 4175 (2010). https://doi.org/10.1002/adfm.201001391

[18]. S. Kumar, A.K. Ojha and B. Walkenfort, J. Photochem. Photobiol. B. Bio. **159**, 111 (2016). https://doi.org/10.1016/j.jphotobiol.2016.03.025

[19]. A.C. Jeoffrey, S.J. Ramalingam, K. Murugaiah and A.R. Balu, Chem. Phys. Impact. **6**, 100246 (2023). https://doi.org/10.1016/j.chphi.2023.100246

[20]. D.S. Pattanayak, J. Mishra, J. Nanda, P.K. Sahoo, R. Kumar and N.K. Sahoo, J. Environ. Mgmt. **297,** 113312 (2021). https://doi.org/10.1016/j.jenvman.2021.113312

[21]. N. Ahmad, S. Sultana, S. Sabir and M.Z. Khan, J. Photochem. Photobiol. A. Chem. **386**, 112129 (2020). https://doi.org/10.1016/j.jphotochem.2019.112129

[22]. M.E. Khan, M.M. Khan and M.H. Cho, J. Coll. Interface Sci. **482,** 221 (2016). https://doi.org/10.1016/j.jcis.2016.07.070

[23]. S.L. Yang, G. Li, J. Feng, P.Y. Wang and L.B. Qu, Electrochim. Acta. **412**, 140157 (2022). https://doi.org/10.1016/j.electacta.2022.140157

[24]. B. Pandit, G.K. Sharma and G.R. Sankapal, J. Coll. Interface Sci. **505**, 1011 (2017). https://doi.org/10.1016/j.jcis.2017.06.092

[25]. A.F. De Faria, D.S.T. Martinez, S.M.M. Meira, A.C.M. De Morales, A. Brandelli, A.G.S. Filho and O.I. Alves, Coll. Surf. B. Interfaces. **113**, 115 (2014). https://doi.org/10.1016/j.colsurfb.2013.08.006

[26]. A. Jarosz, M. Skoda, I. Dudek and D. Szukiewicz, Oxidative Med. Cell. Longev. **2016**, 5851035 (2015).https://doi.org/10.1155/2016/5851035

[27]. H.Z. Zhang, C. Zhang, G.M. Zeng, J.L. Gong, X.M. Ou and S.Y. Huan, J. Coll. Interface Sci. **471**, 94 (2016). https://doi.org/10.1016/j.jcis.2016.03.015"